AIAA JOURNAL
Vol. 33, No. 7, July 1995

# Modeling Considerations for In-Phase Actuation of Actuators Bonded to Shell Structures

Frederic Lalande,* Zaffir Chaudhry,† and Craig A. Rogers‡
*Virginia Polytechnic Institute and State University, Blacksburg, Virginia 24061*

**A closed-form model to represent the in-phase actuation of induced strain actuators bonded to the surface of a circular shell is developed. Because of the inherent shell curvature, the equivalent discrete tangential forces generally used to represent the in-phase actuation of the actuators (such as in pin-force models) are not colinear and result in the application of rigid body forces on the shell. This nonequilibrium state violates the principle of self-equilibrium of fully integrated structures, such as piezoelectrically actuated shells. The solution to this nonequilibrium problem is to apply a uniform transverse pressure over the actuator region to maintain equilibrium. Using this adequate equivalent loading scheme for in-phase actuation, a response model for a circular ring is derived based on shell governing equations. To verify the in-phase actuation response model, finite element analysis is performed. A perfect match between the in-phase actuation response model and the finite elements results, when the actuator mass and stiffness are neglected, validates the derived analytical model. If the self-equilibrium is not maintained (point-force model), the predicted deformed shape is completely different from the actual shell response to in-phase actuation. Thus, by simply applying a uniform transverse pressure along with the discrete tangential forces to maintain the self-equilibrium of the shell, the shell response can be modeled accurately.**

## Introduction

PIEZOELECTRIC (PZT) actuators have been used for active shape, vibration, and acoustic control of structures because of their adaptability and light weight. Their ability to be easily integrated into structures makes them very attractive in structural control since all moving parts encountered with conventional actuators are eliminated. Structural control is obtained by simply embedding PZT actuators in the structure or bonding them on the structure. In structural control, the desired deformation in the structure is obtained by the application of localized line forces and moments generated by the expanding or contracting bonded or embedded PZT actuators. In the case of vibration and acoustic control, the piezoelectric actuators, by the application of these line forces, will change the impedance of the structure to reduce the unwanted dynamic effects at given frequencies.

Previous research performed on PZT-actuated beam and plate structures has led to models describing their response.[1-6] Simple but efficient models were proposed to describe the response of a plate structure to bonded/embedded piezoelectric actuators.[7] By simply replacing the PZT actuator with line forces and moments along its edges, very accurate results are produced even though this type of model is approximate since the mass and stiffness of the actuator is not considered. However, much less research has been done on structures with curvature. Some experimental work[8] and adaptations of flat structure models to curved structures have been made.[9,10] Some models based on shell equations have also been proposed.[11-14]

In a recent paper, Chaudhry et al.[15] considered the modeling of piezoelectric-actuator patches on circular cylinders. When the piezoelectric actuators are actuated in phase, it is found that the point-force model used to represent the actuator creates a rigid body motion since the equivalent line forces are not collinear due to the curvature of the shell (Fig. 1). Since the PZT actuators are integrated within the structure, self-equilibrium must be satisfied. This equilibrium discrepancy between the actual structure and the equivalent loading scheme will produce serious errors when the shell response, based on the line-force representation of the actuator, is calculated. Until now, no models have taken account of this nonequilibrium application of the equivalent line forces. The solution proposed to solve this problem is to apply a uniform transverse pressure over the actuator location to eliminate the rigid body mode. Good agreement between the equivalent loading model and the actual response of the piezoelectrically actuated structure was found.

In this paper, a model for in-phase actuation response of a piezoelectrically actuated circular ring, which takes into account the noncollinear equivalent line forces, is proposed.

## Shell Equivalent Loading Model

The first step in this paper is to repeat the conclusions established by Chaudhry et al.[15] In that paper, an equivalent loading scheme for shell structures was presented. It was shown that in the case of in-phase actuation, a rigid body mode was present due to the fact that the equivalent line forces $L_\theta$ are not collinear (Fig. 1).

To eliminate this nonequilibrium state of the structure, a transverse uniform pressure is added (Fig. 2). The magnitude of the transverse pressure from simple statics is then

$$\bar{p}_r = -(\bar{L}_\theta/a) \tag{1}$$

where

$$\bar{L}_\theta = \frac{E_s t_s}{1-\nu}\frac{2}{2+\psi}\Lambda \tag{2}$$

and

$$\psi = E_s t_s / E_a t_a \tag{3}$$

when the Poisson's ratio of the shell and the piezoelectric actuator are assumed to be the same. $E$, $t$, $L$, and $a$ are the Young's modulus, the thickness, the free induced strain, and the radius of the ring, respectively, whereas the subscripts $s$ and $a$ are the shell and actuator, respectively. If a circular ring is considered, the Poisson's effect disappears since there are no constraints in the axial direction. Thus, for the case of a ring, the Poisson's ratio in Eq. (2) is set to zero. Based on this equivalent loading scheme, a response model for a circular ring with two discrete tangential forces and a uniform radial pressure will be derived.

Presented as Paper 94-1779 at the AIAA/ASME/ASCE/AHS/ASC 35th Structures, Structural Dynamics, and Materials Conference, Hilton Head, SC, April 18–20, 1994; received May 9, 1994; revision received Sept. 21, 1994; accepted for publication Sept. 22, 1994. 

*Senior Graduate Research Assistant, Center for Intelligent Material Systems and Structures. Student Member AIAA.

†Research Scientist, Center for Intelligent Material Systems and Structures. Member AIAA.

‡Professor and Director, Center for Intelligent Material Systems and Structures. Member AIAA.

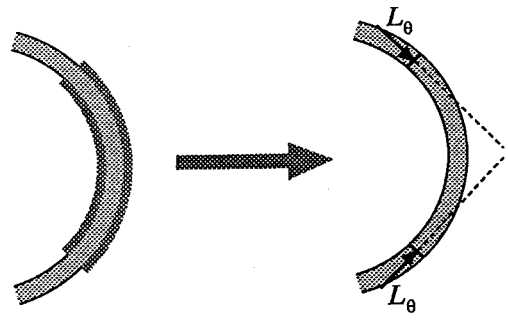


**Fig. 1 Nonequilibrium of discrete tangential forces in shell structures.**

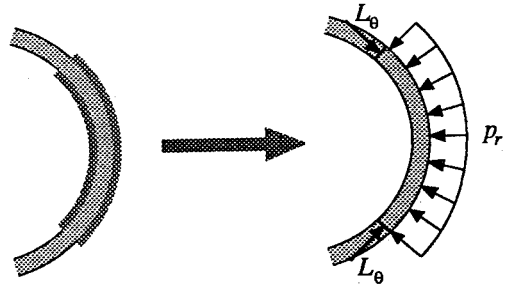


**Fig. 2 Adequate equivalent loading to maintain equilibrium.**

## Derivation of Governing Equations

A brief overview of the governing equations of a thin ring subjected to radial pressure and discrete tangential loading will be presented.[16] In the case of a thin circular ring, only the in-plane stress resultants $N_\theta$, $M_\theta$, and $Q_{\theta r}$ are present, and a linear variation in the transverse direction and a constant radial displacement through the thickness are assumed (Kirchhoff's assumption[16]):

$$v = v^0 + z\beta \tag{4a}$$

$$w = w^0 \tag{4b}$$

$$\beta = \frac{1}{a}\left(v^0 - \frac{\partial w^0}{\partial \theta}\right) \tag{4c}$$

where $\beta$ is the rotational displacement and $v^0$ and $w^0$ are the neutral surface tangential and radial displacements, respectively.

Under these assumptions, the strain-displacement relation is

$$\varepsilon_\theta = \frac{1}{a}\left(\frac{\partial v^0}{\partial \theta} + w^0\right) + \frac{z}{a^2}\left(\frac{\partial v^0}{\partial \theta} - \frac{\partial^2 w^0}{\partial \theta^2}\right) \tag{5}$$

The membrane force, bending moment, and transverse shear force resultants are obtained by integrating the stress components through the thickness of the ring

$$N_\theta = \int_{-t_s/2}^{t_s/2} \sigma_\theta \, dz = \int_{-t_s/2}^{t_s/2} E\varepsilon_\theta \, dz = \frac{K}{a}\left(\frac{\partial v^0}{\partial \theta} + w^0\right) \tag{6a}$$

$$M_\theta = \int_{-t_s/2}^{t_s/2} \sigma_\theta z \, dz = \int_{-t_s/2}^{t_s/2} E\varepsilon_\theta z \, dz = \frac{D}{a^2}\left(\frac{\partial v^0}{\partial \theta} - \frac{\partial^2 w^0}{\partial \theta^2}\right) \tag{6b}$$

$$Q_{\theta r} = \int_{-t_s/2}^{t_s/2} \sigma_{\theta r} \, dz \tag{6c}$$

where the membrane and bending stiffnesses are

$$K = Et_s \tag{7a}$$

$$D = Et_s^3/12 \tag{7b}$$

respectively. It must be noted that the Poisson's ratio is not present in the stiffness expressions Eq. (7) since the ring is free of deform in the axial direction.

The equilibrium equations derivation is based on the energy method, using Hamilton's principle

$$\int_{t_0}^{t_1} [\delta(U - E_b - E_L) - \delta K] \, dt = 0 \tag{8}$$

where $\delta(U - E_b - E_L)$ is the total variational potential energy and $\delta K$ is the variational kinetic energy. Since the ring is subjected to static loading, the kinetic energy term is equal to zero. The Love ring equations for the equivalent loading scheme are found to be

$$\frac{dN_\theta(\theta)}{a\,d\theta} + \frac{1}{a}\frac{dM_\theta(\theta)}{a\,d\theta} + \frac{\bar{L}_\theta}{a}\delta(\theta - \theta_p) = 0 \tag{9a}$$

$$\frac{d^2M_\theta(\theta)}{a^2\,d\theta^2} - \frac{N_\theta(\theta)}{a} + p_r(\theta) = 0 \tag{9b}$$

The derived equilibrium equations [Eq. (9)] are very similar to those obtained when a pressure loading is considered. The difference appears in the tangential line loading term $(\bar{L}_\theta/a)\delta(\theta - \theta_p)$ which replaces the $p_\theta(\theta)$ term when tangential pressure loading is considered.

Indeed, this difference occurs in the potential energy of the external line loading used in Hamilton's principle, which is given by

$$E_L = \int_x \bar{L}_\theta v^0 \, dx \tag{10}$$

Rewriting the previous equation under a double integral by introducing a Dirac function

$$E_L = \int_x \int_\theta \left(\frac{\bar{L}_\theta}{a}\delta(\theta - \theta_p)v^0\right) a \, d\theta \, dx \tag{11}$$

where $\theta_p$ is the location of the applied line load. The loads are assumed to be applied on the neutral surface of the ring.

Finally, the necessary boundary conditions for the ring are

$$N_\theta = N_\theta^* \quad \text{or} \quad v^0 = v^{0*} \tag{12a}$$

$$M_\theta = M_\theta^* \quad \text{or} \quad \beta = \beta^* \tag{12b}$$

and

$$Q = Q^* \quad \text{or} \quad w^0 = w^{0*} \tag{12c}$$

## Derivation of the In-Phase Actuation Response Model

With the governing equations now derived, the next step is to apply them to the particular problem shown in Fig. 3. To simplify the analytical model derivation, the actuator stiffness will be neglected.

As established previously, the ring is subjected to discrete tangential forces at the end of the modeled actuator and to a uniform radial pressure of magnitude $(\bar{L}_\theta/a)$ Eq. (1), to ensure equilibrium

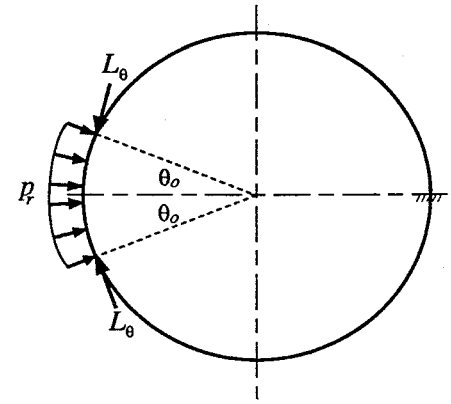


**Fig. 3 Adequate equivalent actuator loading on the ring.**

of the ring. The loading of the ring is expressed using Dirac and Heaviside functions

$$L_\theta(\theta) = \bar{L}_\theta[\delta^- - \delta^+] \tag{13}$$

$$p_r(\theta) = \bar{p}_r[H^- - H^+] = -(\bar{L}_\theta/a)[H^- - H^+] \tag{14}$$

where

$$\theta^- = \theta - (\pi - \theta_0) \tag{15a}$$

$$\theta^+ = \theta - (\pi + \theta_0) \tag{15b}$$

$$\delta^- = \delta[\theta^-] \tag{16a}$$

$$\delta^+ = \delta[\theta^+] \tag{16b}$$

$$H^- = H[\theta^-] \tag{17a}$$

$$H^+ = H[\theta^+] \tag{17b}$$

The integration constants will be determined from the continuity conditions at $\theta = 0, 2\pi$

$$w^0(0) = w^0(2\pi) \tag{18a}$$

$$v^0(0) = v^0(2\pi) \tag{18b}$$

$$\beta(0) = \beta(2\pi) \tag{18c}$$

From the rotational displacement expression Eq. (4c), it is possible to rewrite the continuity conditions of Eq. (18c), by making use of Eq. (18a), as

$$w'^0(0) = w'^0(2\pi) \tag{18d}$$

Combining the equilibrium equations Eq. (9), the differential equation for the moment in the ring is obtained as follows:

$$\frac{\mathrm{d}^3 M_\theta(\theta)}{\mathrm{d}\theta^3} + \frac{\mathrm{d}M_\theta(\theta)}{\mathrm{d}\theta} = -a^2\left[\frac{L_\theta(\theta)}{a} + p_r'(\theta)\right] = 0 \tag{19}$$

Substituting the loading expressions Eqs. (13) and (14) in the previous equation [Eq. (19)], it can be seen that the right-hand side of the equation will be zero. Solving the differential equation [Eq. (19)], an expression of the moment distribution in the ring is obtained

$$M_\theta(\theta) = C_1 + C_2 \sin\theta + C_3 \cos\theta \tag{20}$$

Combining the two stress-displacement equations Eqs. (6), the following differential equation is obtained:

$$w^0(\theta) + \frac{\mathrm{d}^2 w^0(\theta)}{\mathrm{d}\theta^2} = \frac{a^2}{D}\left(\frac{N_\theta(\theta)D}{Ka} - M_\theta(\theta)\right) \tag{21}$$

Rewriting the second equilibrium equation [Eq. (9b)],

$$N_\theta(\theta) = \frac{1}{a}\frac{\mathrm{d}^2 M_\theta(\theta)}{\mathrm{d}\theta^2} + a p_r(\theta). \tag{22}$$

Substituting the expression of the moment Eq. (20) and the tangential force Eq. (22) into Eq. (21), the following differential equation in $w^0(\theta)$ is obtained:

$$w^0(\theta) + \frac{\mathrm{d}^2 w(\theta)}{\mathrm{d}\theta^2} = -\frac{a^2}{D}\left[C_1 + C_2\left(1 + \frac{D}{Ka^2}\right)\sin\theta + C_3\left(1 + \frac{D}{Ka^2}\right)\cos\theta - \frac{D}{K}p_r(\theta)\right] \tag{23}$$

For thin rings, the $D/Ka^2$ term is neglected since its value is much less than one. The radial-displacement equation is obtained using Laplace transform

$$w^0(\theta) = \frac{a^2}{D}\Bigg[C_1(1-\cos\theta) + \frac{C_2}{2}(\sin\theta - \theta\cos\theta) + \frac{C_3}{2}(\theta\sin\theta) + \frac{D\bar{p}_r}{K}[(1-\cos\theta^-)H^- - (1-\cos\theta^+)H^+] + w^0(0)\cos\theta + w^{0\prime}(0)\sin\theta\Bigg] \tag{24}$$

Introducing Eq. (24) in Eq. (6a), the tangential displacement differential equation is

$$\frac{\mathrm{d}v^0(\theta)}{\mathrm{d}\theta} = \frac{a^2}{D}\Bigg\{-C_1(1-\cos\theta) - \frac{C_2}{2}(\sin\theta - \theta\cos\theta) - \frac{C_3}{2}(\theta\sin\theta) + \frac{D\bar{p}_r}{K}[\cos\theta^- H^- - \cos\theta^+ H^+] - w^0(0)\cos\theta - w^{0\prime}(0)\sin\theta\Bigg\} \tag{25}$$

Solving this equation using Laplace transformation and applying continuity conditions Eq. (18), the equations of the tangential and radial displacements are found to be

$$v^0(\theta) = \frac{a^2\bar{p}_r}{K}\Bigg\{-\frac{\sin\theta_0}{\pi}(\sin\theta - \theta\cos\theta) + [\sin\theta^- H^- - \sin\theta^+ H^+]\Bigg\} \tag{26}$$

and

$$w^0(\theta) = \frac{a^2\bar{p}_r}{K}\Bigg\{\frac{\sin\theta_0}{\pi}\theta\sin\theta + [(1-\cos\theta^-)H^- - (1-\cos\theta^+)H^+]\Bigg\} \tag{27}$$

## Finite Element Verification

The developed in-phase actuation response model is verified using finite element analysis. A ring of 6 in. radius, 0.032 in. thickness and 1 in. deep, and piezoelectric actuators 1/6 of the ring thickness and covering an arc 30 deg long ($2\theta_0$), are used. A Young modulus of 30 Msi and 9.1 Msi are used for the ring and the PZT actuators, respectively. Making use of symmetry, the finite element model consists of beam elements in the upper-half of the ring only, as shown in Fig. 4. Two load cases are considered: 1) temperature contraction equivalent to 1000 $\mu$strain of the beam elements modeling the actuator region and 2) equivalent discrete forces and uniform pressure loading from Eqs. (1) and (2). The finite element analysis results are shown in Fig. 5, as well as the in-phase actuation response model results. A single curve can be observed since the curves match perfectly. Also shown in Fig. 5 are the displacements of the same ring if

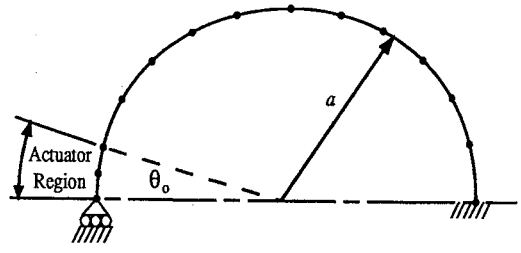


**Fig. 4 Finite element model using beam elements.**

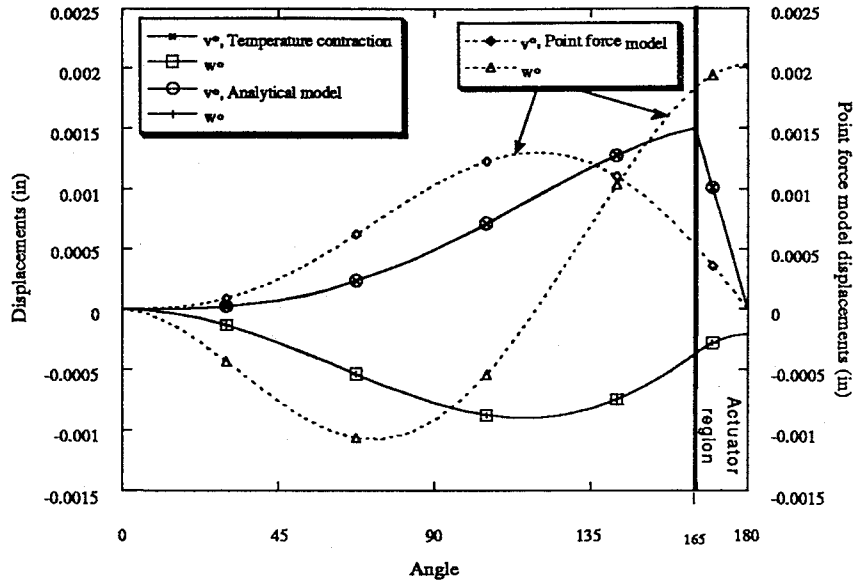


**Fig. 5 Match of displacements between the analytical model and the finite element model using beam elements.**

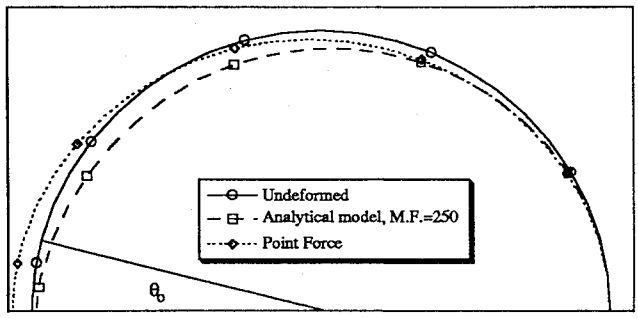


**Fig. 6 Deformed shape of the ring with and without self-equilibrium loading.**

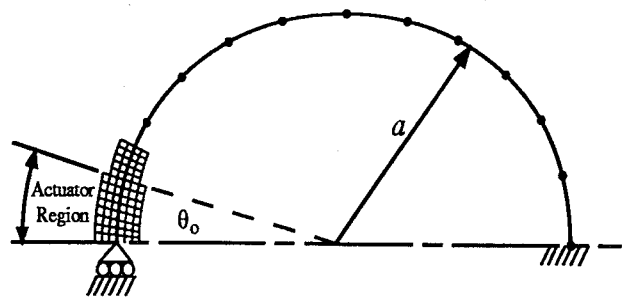


**Fig. 7 Finite element model using plane stress elements.**

only discrete tangential forces are applied (point-force model). The point-force model does not satisfy the ring's self-equilibrium. Major displacement discrepancies between the in-phase actuation response and the point-force model occur both in shape and magnitude. The point-force model overpredicts the displacements by a factor up to 1000. Figure 6 shows the deformed shape of the self-equilibrium loading and the nonequilibrium loading with the displacements magnified by a 250 and 1 factor, respectively. It can be seen again that when a uniform pressure is not applied to maintain equilibrium, the deformed shape is erroneous. Also, a reaction force in the $x$ direction at the clamped boundary condition is present if the uniform pressure is not applied. This reaction force should not be present since the actual ring with bonded actuators is in self-equilibrium. The adequate equivalent loading did not show any reaction force in the $x$ direction at the clamped boundary condition. The verification of the results also have been made with 10-deg- and 60-deg-long piezoelectric patches, and the coincidence is still perfect between the in-phase actuation response model and the finite element analysis.

However, it must be mentioned that the response of the ring is very sensitive to the applied load in the finite element model. An error of 0.1% in the magnitude of the applied equivalent line force will completely change the response of the ring. This sensitivity of the nodal displacements is due to the low stiffness of the ring (0.032 in. thick only). The application of a tangential line force of 0.1% magnitude of the applied equivalent line force on the ring will produce nodal displacements of the same order as the self-equilibrium loading nodal displacements.

Also, the pressure loading must be transformed to nodal forces only (lumped loading). The lumped loading is often better for flat elements representing a curved surface.[17]

Up to this point, the added stiffness of the actuators has been neglected both in the analytical model and the finite element analysis. A second finite element model, using plane stress elements in the actuator region to include the actuator's stiffness, is made to compare the actual behavior of the system to the derived analytical model (Fig. 7). To keep finite element model small, the actuator size is reduced to 10 deg ($2\theta_0$). The radial and tangential displacements are shown in Fig. 8. Disparities between the analytical model and the plane stress finite element model are present since the actuator stiffness is not neglected and no assumptions toward equivalent loading are made on the latter one. Increased actuator stiffness will further increase the disparities between the two solutions. But, it should be borne in mind that in typical applications the actuator patches are small and add minimally to the baseline structural stiffness. Even though displacement differences are present, the plane stress finite element model validates the derived analytical model since it gives results of the same order of magnitude with similar deformed shapes as opposed to the point-force model previously discussed. The deformed shape of the analytical model and the plane stress finite element model is shown in Fig. 9.

The discussion of in-phase actuation of induced strain actuators symmetrically bonded on shells can be extended to unsymmetric actuation. Unsymmetric actuation is obtained when the actuators on each side of the shell are submitted to voltage of different magnitudes, or when a single actuator is bonded on one side of the shell. Unsymmetric actuation is a combination of extension and bending of the shell and can be solved using simple superposition. Thus, for unsymmetric actuation, the equivalent loading will consist of discrete tangential forces and moments at the ends of the actuator(s) and a distributed transverse pressure over the actuator(s) footprint to maintain the self-equilibrium of the shell.

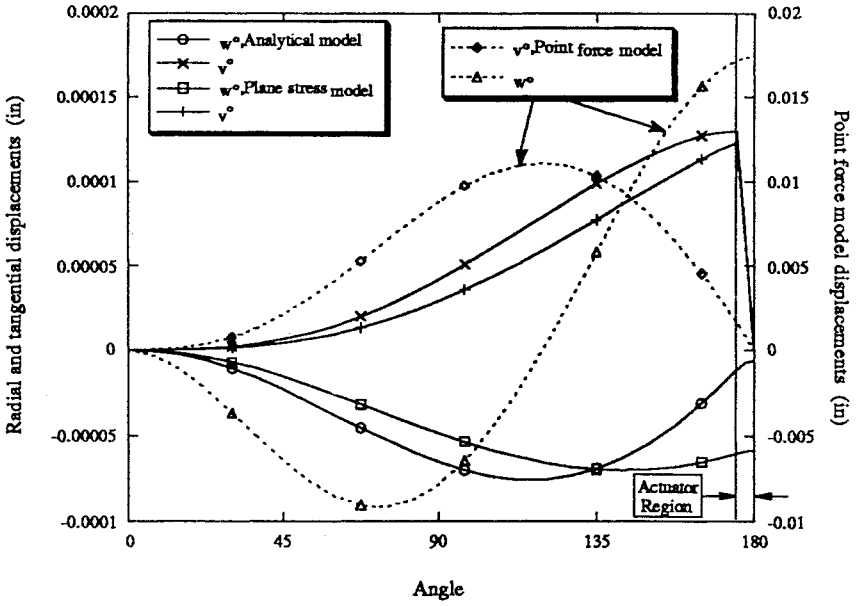


**Fig. 8 Match of displacements between the analytical model and the finite element model using plane stress elements.**

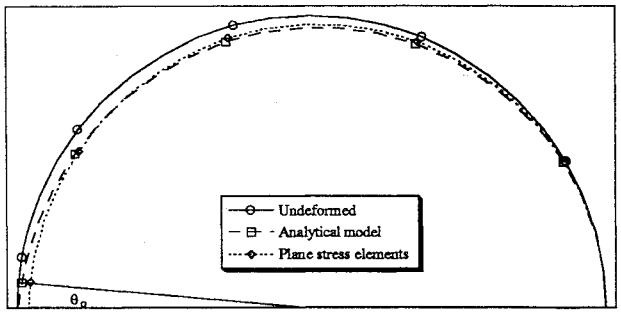


**Fig. 9 Deformed shape of the ring using the self-equilibrium loading and the plane stress elements.**

## Conclusion

In this paper, a closed-form solution for a ring subjected to in-phase actuation of surface bonded strain actuators is presented. The loading used to represent the in-phase actuation consists of uniform transverse pressure and tangential line forces to maintain the self-equilibrium of the shell structure. The results of the in-phase actuation deformation model are in exact agreement with the finite elements results when actuator stiffness is neglected. If the actuator stiffness is considered, the analytical model gives a good approximation of the shell's deformed shape. If the self-equilibrium is not maintained (point-force model), the predicted deformed shape is completely different from the actual shell response to in-phase actuation. Thus, a uniform transverse pressure in addition to the tangential line loads is necessary to preclude rigid body motion and to obtain accurate displacement response.

## Acknowledgments

The authors would like to acknowledge the funding support of the Office of Naval Research, Grant ONR N00014-92-J-1170, Kam Ng, Technical Monitor.

## References

[1]Crawley, E. F., and de Luis, J., "Use of Piezoelectric Actuators as Elements of Intelligent Structures," *AIAA Journal*, Vol. 25, No. 10, 1987, pp. 1373–1385.

[2]Crawley, E. F., and Anderson, E. H., "Detailed Models of Piezoceramic Actuation of Beams," *Journal of Intelligent Material Systems and Structures*, Vol. 1, No. 1, 1990, pp. 4–25.

[3]Dimitriadis, E. K., Fuller, C. R., and Rogers, C. A., "Piezoelectric Actuators for Distributed Vibration Excitation of Thin Plates," *Journal of Vibration and Acoustics*, Vol. 113, Jan. 1991, pp. 100–107.

[4]Liang, C., Sun, F. P., and Rogers, C. A., "An Impedance Method for Dynamic Analysis of Active Material Systems," *Proceedings of the AIAA/ASME/ASCE/AHS/ASC 34th Structures, Structural Dynamics, and Material Conference* (La Jolla, CA), AIAA, Washington, DC, April 1993, pp. 3587–3599 (AIAA Paper 93-1713).

[5]Wang, B. T., and Rogers, C. A., "Modeling of Finite-Length Spatially Distributed Induced Strain Actuators for Laminate Beams and Plantes," *Proceedings of the AIAA/ASME/ASCE/AHS/ASC 32th Structures, Structural Dynamics, and Material Conference* (Baltimore, MD), AIAA, Washington, DC, 1991, pp. 1511–1520 (AIAA Paper 91-1258).

[6]Zhou, S., Liang, C., and Rogers, C. A., "A Dynamic Model of a Piezoelectric Actuator Driven Thin Plate," *Proceedings of the Society of Photo-Optical Instrumental Engineers North American Conference on Smart Structures and Materials* (Orlando, FL), SPIE, Bellingham, WA, 1994, pp. 550–562.

[7]Crawley, E. F., and Lazarus, K. B., "Induced Strain Actuation of Isotropic and Anisotropic Plates," *AIAA Journal*, Vol. 29, No. 6, 1989, pp. 944–951.

[8]Fuller, C. R., Snyder, S., Hanson, C., and Silcox, R., "Active Control of Interior Noise in Model Aircraft Fuselages using Piezoceramic Actuators," *Proceedings of the AIAA 13th Aeroacoustic Conference* (Tallahassee, FL), AIAA, Washington, DC, 1990 (AIAA Paper 90-3922).

[9]Lester, H. C., and Lefebvre, S., "Piezoelectric Actuator Models for Active Sound and Vibration Control of Cylinders," *Proceedings of the Recent Advances in Active Noise and Vibration Control Conference* (Blacksburg, VA), Technomic Publishing Co., Lanscaster, PA, 1991, pp. 3–26.

[10]Sonti, V. R., and Jones, J. D., "Active Vibration Control of Thin Cylindrical Shells using Piezoelectric Actuators," *Proceedings of the Recent Advances in Active Noise and Vibration Control Conference*, Blacksburg, VA, Technomic Publishing Co., Lanscaster, PA, 1991, pp. 27–38.

[11]Larson, P. H., and Vinson, J. R., "The Use of Piezoelectric Materials in Curved Beams and Rings," *Proceedings of the American Society of Mechanical Engineers Winter Annual Meeting* (New Orleans, LA), ASME Technical Publishing, New York, 1993, pp. 277–285.

[12]Rossi, A., Liang, C., and Rogers, C. A., "Impedance Modeling of Piezoelectric Actuator-Driven Systems: an Application to Cylindrical Ring Structures," *Proceedings of the AIAA/ASME/ASCE/AHS/ASC 34th Structures, Structural Dynamics, and Material Conference* (La Jolla, CA), AIAA, Washington, DC, 1993, pp. 3618–3624 (AIAA Paper 93-1716).

[13]Sonti, V. R., and Jones, J. D., "Curved Piezo-Actuator Models for Active Vibration Control of Cylindrical Shells," Proceedings of the 125th Meeting of the Acoustical Society of America, Ottawa, Canada, May 17–21.

[14]Zhou, S., Liang, C., and Rogers, C. A., "Impedance Modeling of Two Dimensional Piezoelectric Actuators Bonded on a Cylinder," *Proceedings of the American Society of Mechanical Engineers Winter Annual Meeting* (New Orleans, LA), ASME Technical Publishing, New York, 1993, pp. 247–255.

[15]Chaudhry, Z., Lalande, F., and Rogers, C. A., "Modeling of Induced Strain Actuator Patches," *Proceedings of the Society of Photo-Optical Instrumentation Engineers North American Conference on Smart Structures and Materials* (Orlando, FL), SPIE, Bellingham, WA, 1994, pp. 563–570.

[16]Soedel, W., *Vibrations of Plates and Shells*, Marcel and Decker, New York, 1981, pp. 9–41.

[17]De Salvo, G. J., and Swanson, J. A., ANSYS User's Manual, Swanson Analysis Systems, Houston, PA, 1979.